HHS Public Access

Author manuscript

Adv Biol (Weinh). Author manuscript; available in PMC 2024 May 01.

Published in final edited form as:

Adv Biol (Weinh). 2023 May ; 7(5): e2200160. doi:10.1002/adbi.202200160.

DNA methylation dynamics during esophageal epithelial regeneration following repair with acellular silk fibroin grafts in rat

Lauren A. Urban[1,4], **Jiachun Li**[2,†], **Gokhan Gundogdu**[3,†], **Annie Trinh**[1,4,5,†], **Hanjuan Shao**[2,4], **Travis Nguyen**[2], **Joshua R. Mauney**[2,3,*], **Timothy L. Downing**[1,2,4,5,*]

[1]Department of Microbiology & Molecular Genetics, University of California Irvine; Irvine, California, USA

[2]Department of Biomedical Engineering, University of California, Irvine, Irvine, CA, 92697, USA

[3]Department of Urology, University of California, Irvine, Orange, CA, 92868, USA

[4]UCI Edwards Lifesciences Foundation Cardiovascular Innovation and Research Center (CIRC), University of California-Irvine, Irvine, CA 92697, USA

[5]The NSF-Simons Center for Multiscale Cell Fate Research, University of California-Irvine, Irvine, California 92697, USA

Abstract

Esophageal pathologies such as atresia and benign strictures often require surgical reconstruction with autologous tissues to restore organ continuity. Complications such as donor site morbidity and limited tissue availability have spurred the development of acellular grafts for esophageal tissue replacement. Acellular biomaterials for esophageal repair rely on the activation of intrinsic regenerative mechanisms to mediate de novo tissue formation at implantation sites. Previous research has identified signaling cascades involved in neoepithelial formation in a rat model of onlay esophagoplasty with acellular silk fibroin grafts, including phosphoinositide 3-kinase (PI3K), and protein kinase B (Akt) signaling. However, it is currently unknown how these mechanisms are governed by DNA methylation (DNAme) during esophageal wound healing processes. We performed reduced-representation bisulfite sequencing to characterize temporal DNAme dynamics in host and regenerated tissues up to 1-week post-implantation. Overall, we observe global hypermethylation at post-reconstruction timepoints and an inverse correlation between promoter DNAme and the expression levels of differentially expressed proteins during regeneration. Site-specific hypomethylation targets genes associated with immune activation while

*Corresponding authors: tim.downing@uci.edu, mauneryj@hs.uci.edu.

†These authors contributed equally

AUTHOR CONTRIBUTIONS

T.L.D., J.R.M., and G.G. conceived of and designed the study. J.R.M., G.G., and T.N. oversaw and performed the animal experiments. H.S. performed RRBS library preparation and submitted samples to UC Irvine's Genomics High-Throughput Facility (GHTF) for sequencing. L.A.U., J.L., and A.T. performed the bioinformatic analyses and prepared the figures. L.A.U, J.L., A.T., J.R.M. and T.L.D. interpreted the data and wrote the manuscript with assistance from the other authors.

COMPETING INTEREST

J.R.M is a co-inventor on the patented BLSF technology, paid consultant and co-founder of WeaveTech Corporation. G.G. is also a paid consultant for WeaveTech Corporation.

hypermethylation occurs within gene bodies encoding PI3K-Akt signaling components during the tissue remodeling period. Our data provide insight into the epigenetic mechanisms during esophageal regeneration following surgical repair with acellular grafts.

Graphical Abstract

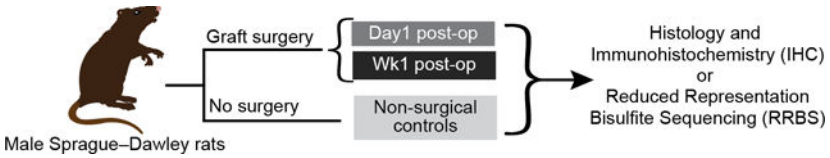

This work characterizes DNA methylation changes during esophageal regeneration in rats after surgical repair with acellular grafts. CpG methylation modulates the transcriptional activity of genes. Decreases in CpG methylation target genes involved in immune activation, while site-specific increases in CpG methylation target genes encoding components of the PIK3-Akt signaling pathway.

Keywords

DNA methylation; epigenetics; acellular grafts; esophagus; tissue regeneration

1 Introduction

Congenital and acquired disorders of the esophagus including atresia, stricture disease, and malignancies often require surgical reconstruction of focal or tubular esophageal segments with autologous tissue grafts to reestablish organ continuity and restore tissue function. [1–4] However, this gold standard approach is frequently hampered by complications such as donor site morbidity and limited donor tissue availability, [5] which has spurred research into the development of acellular biomaterials for esophageal tissue engineering. [6] Bi-layer silk fibroin (BLSF) scaffolds represent an emerging platform for esophageal repair due to their high structural strength and elasticity, low immunogenicity, and tunable degradative properties, [7] These matrices have been previously demonstrated to support the formation of innervated, vascularized esophageal tissues with contractile properties sufficient for solid food ingestion in preclinical animal models. [7,8] Constructive remodeling of BLSF scaffolds is dependent on the ability of host progenitor cell populations to migrate, proliferate, and differentiate within the implant microenvironment to facilitate regeneration of functional neotissues. [7] Molecular mechanisms governing scaffold-mediated wound healing processes in the esophagus are largely unexplored. An increased understanding of regenerative signaling networks and their regulation may allow for the development of instructive biomaterial designs to maximize esophageal repair outcomes.

Recent reports from our research team utilized quantitative proteomics and in silico pathway evaluations to identify signaling cascades which were significantly activated/inhibited during neoepithelial regeneration in a rat model of onlay esophagoplasty with BLSF grafts. [8] Pharmacologic inhibitor and rescue experiments demonstrated that epithelialization of esophageal neotissues is significantly dependent in part on pro-survival stimuli capable of

suppressing caspase activity in epithelial progenitors via activation of hepatocyte growth factor receptor (c-MET), tropomyosin receptor kinase A (TrkA), phosphoinositide 3-kinase (PI3K), and protein kinase B (Akt) signaling pathways. Interestingly, activation of these pro-survival signaling cascades in cancer cells is largely influenced by epigenetic mechanisms, such as DNA methylation (DNAme) which occurs in mammals most commonly in the context of CpG dinucleotides. [9] For example, a loss of DNAme at a CpG island associated with the activation of oncogene *PIK3CA* expression, which encodes a catalytic subunit of PI3K, is thought to play a part in activating the PI3K/Akt pathway and contributing to tumorigenesis in esophageal cancer patients. [10] Altered DNAme signatures of genes encoding integral components of c-MET and TrkA signaling pathways have also been reported to be key drivers of various malignancies. [11,12] The involvement of DNAme in these pathways, which are also essential to regenerative and wound healing responses, [13–15] alludes to the potential role of DNAme in facilitating cell fate and lineage decisions in esophageal neotissues. However, the role of DNAme in esophageal tissue regeneration following surgical reconstruction remains poorly understood.

In this present study, we aimed to characterize the DNAme changes which occur following surgical injury and neoepithelial formation in rat esophageal tissues subjected to onlay esophagoplasty with BLSF grafts. Specifically, we performed reduced-representation bisulfite sequencing (RRBS) to profile the DNAme landscape in host and regenerated tissues up to 1 week post-operatively, identified CpGs which undergo differential methylation in response to tissue damage and repair, and elucidated putative biological processes associated with DNAme alterations.

2 Results

2.1 RRBS reveals global DNA hypermethylation during surgical reconstruction and regeneration of esophageal tissue

In this study, we performed histological, immunohistochemistry (IHC), and RRBS analysis on rat esophageal tissue that was collected at 1 day (Day1) and 1 week (Wk1) following onlay esophagoplasty with BLSF grafts, as well as from nonsurgical controls (NSC) (Figure 1A and 1B). There were no significant intra-operative or post-operative complications with onlay esophagoplasty procedures and the survival rate was 100% until scheduled euthanasia. Masson's trichrome staining of reconstructed esophageal tissue was performed to temporally characterize the host response and degree of tissue regeneration following scaffold implantation (Figure 1B). Day1 post-op, the BLSF graft was largely intact and the implant site was populated with mononuclear inflammatory cells and neutrophils with limited tissue integration from the host esophagus. At Wk1 post-op, an epithelialized fibrovascular scar composed of mononuclear inflammatory and fibroblastic cell types was evident within the original graft site (Figure 1B).

We performed immunohistochemistry (IHC) staining for the three major mammalian DNA methyltransferases DNMT1, 3A, and 3B protein expression which revealed the presence of all 3 methyltransferases in NSC and reconstructed host tissues at Day1 and Wk1 after surgery. DNMT3B expression was primarily nuclear and was detected in epithelial, mucosal, and skeletal muscle compartments throughout NSC and reconstructed tissues NSC

(Figure 1C). In contrast, NSC tissues displayed both cytoplasmic and nuclear DNMT1 and DNMT3A expression which was mainly localized to CK5+FG- basal epithelial cells. Qualitative increases in cytoplasmic expression of these markers were also observed in host and regenerated epithelia at Day1 and Wk1, respectively, in comparison to NSC (Figure 1C).

To characterize CpG methylation during regeneration we performed RRBS on genomic DNA extracted from harvested rat esophageal tissues and sequenced reads were aligned to the rat genome (mRATBN7.2/rn7) using Bismark (see Experimental Section). On average, we captured 14.7 million CpGs with >70% mapping efficiency per sample which is consistent with previous RRBS reports in rat (Figure S1A; Additional file 1: Table S1A). Methylation calls were performed with Bismark (see Experimental Section) [16]. To compare global patterns of site-specific CpG methylation during regeneration, CpGs were filtered for ≥5x coverage. We identified a significant increase in the percentage of methylated CpGs captured at Day1 relative to the NSC condition (p=0.016) (Figure 1D; Additional file 1: Table S1B). DNAme levels decreased between Day1 and Wk1, however this difference was not significant (p=0.19). DNAme levels at Wk1 compared to the NSC condition were not significantly different (p=0.11). This result suggests that esophageal tissues undergo a gain in DNAme, or DNA hypermethylation, during regeneration which may be a transient response immediately following surgical repair as methylation levels appear to trend towards baseline (NSC) levels by Wk1 post-op.

Of the captured CpGs, a total of 514,813 unique CpG sites were captured in ≥3 replicates in all conditions and used in downstream analyses. These CpGs fell within intergenic regions (40.1%), introns (43%), promoters (24.6%), and exons (21.9%) (Additional file 1: Table S1C). Methylation calls for the total 514,813 CpGs were merged across replicates within each condition. Consistent with our previous global CpG analysis, the distributions of DNAme percentage at each timepoint revealed that Day1 and Wk1 conditions exhibited a greater frequency of highly methylated CpGs (e.g., methylation percentage >80%) relative to the NSC condition (Figure 1E).

2.2 Promoter methylation is inversely correlated with expression level of differentially expressed proteins (DEPs) during regeneration

Previously, we identified a set of differentially expressed proteins (DEPs) that are modulated during regeneration in esophageal tissues following BLSF implant surgery (Figure S1B and S1C; Additional file 1: Table S1D). [8] To better understand the relationship between DEPs and methylation changes, we investigated how methylation levels change in CpGs that fall within genic regions encoding DEPs. Notably, methylation levels were lower in CpGs within promoters and gene bodies that encode upregulated DEPs at Day1 compared to the NSC (Figure S1D and S1E, Additional file 1: Table S1E and S1F). Gene ontology (GO) analysis revealed these genes were enriched for biological processes (BP) associated with immune activation (Figure S1D and S1E, Additional file 1: Table S1G and S1H). This could reflect immune cell infiltration at the graft site which has been observed previously after surgical injury and during wound healing processes. [17]

To characterize differential DNAme during post-surgical reconstruction, we identified a set of differentially methylated CpGs (DMCs) that were determined based on their magnitude

of DNAme changes (≥20% methylation difference) and their significance level ($q<0.05$) between timepoints. We focused initially on identifying DMCs present in post-op samples compared to NSCs (i.e., NSC→Day1, NSC→Wk1). We found that DMCs that fell within promoter of genes encoding DEPs showed an inverse correlation in their methylation difference compared to previously reported changes in protein expression for NSC→Day1 and NSC→Wk1 timepoints ($R=-0.52$ and -0.37 respectively) (Figure 2A; Additional file 1: Table S2A).

We observed a similar, but less apparent inverse correlation for DMCs located within the gene body of genes encoding DEPs (Figure 2B; Additional file 1: Table S2B). We found upregulated DEPs were associated with DNA hypomethylation at NSC→Day1 DMCs that occurred in promoters of genes involved in immune activation such as S100A8 (S100 Calcium Binding Protein A8) and Platelet factor 4 (Pf-4) (Figure 2A). [18] Pf-4 regulates proinflammatory responses in monocytes and macrophages in humans and murine bone marrow-derived macrophages and acts as an inhibitor of angiogenesis. [19,20] The most upregulated DEPs were associated with DNA hypomethylation at NSC→Wk1 DMCs found in the promoters of genes involved in T-cell activation such as Vav Guanine Nucleotide Exchange Factor 1 (VAV1), a critical regulator of signal transduction in T-cells and B-cells, and Proteasome subunit beta type-10 (Psmb10) which forms an immunoproteasome complex involved in histocompatibility complex antigen presentation (Figure 2A). [21]

2.3 While the genome shows global hypermethylation, genic regions contain both hyper and hypomethylated DMCs

We next sought to characterize timepoint-specific changes in DNAme during esophageal regeneration. To do so, we identified DMCs that were uniquely associated to a single two-way timepoint comparison versus those that were shared across multiple two-way timepoint comparisons (Figure 3A). At this resolution, we observed the majority of DMCs were uniquely associated with the NSC→Wk1 condition (n=28,552). The NSC→Day1 condition had the second largest number of uniquely associated DMCs (n=6,120) and the Day1Wk1 condition had the fewest uniquely associated DMCs (n=535). Thus, we focused our downstream analyses on the majority of DMCs which occur between post-surgical timepoint conditions and the NSC (i.e., NSC→Day1 DMCs and NSC→Wk1 DMCs). While there were 135 universally shared DMCs among all three timepoint comparisons, NSC→Day1 and NSC→Wk1 comparisons shared a total of 5,658 DMCs. We found that the majority of DMCs in the NSC→Day1 and NSC→Wk1 conditions were hypermethylated (9,247 and 25,945, respectively) while a substantially smaller subset of DMCs were hypomethylated at these same timepoints (3,032 and 8,561, respectively) (Figure 3B; Additional file 1: Table S3A). The distribution of methylation difference comprising hypermethylated DMCs (HyperDMCs) and hypomethylated DMCs (HypoDMCs), however, appeared comparable across both timepoint comparisons (Figure 3C). To profile DNAme changes among shared DMCs across individual samples, the set of CpGs comprising the 5,658 shared DMCs between NSC→Day1 and NSC→Wk1 was further filtered for CpGs with ≥5x coverage across *all* experimental samples, which resulted in 3,494 CpGs (Figure 3D). Euclidean hierarchical clustering revealed that the data separated according to CpG site dynamics and condition. We found three DNA methylation patterns emerged during regeneration.

We observed >70% of CpGs gained methylation in post-surgical timepoints (Cluster 2 and Cluster 3) while the DMCs in Cluster 1 lost methylation in post-surgical timepoints (Figure 3D). The relative distribution of CpGs captured in each cluster revealed that the majority of DMCs in Cluster 1 and Cluster 3 occur within gene bodies (79% and 57% respectively) and a smaller percentage occur in promoters (14% and 21% respectively). The majority of DMCs in Cluster 2 occur outside of promoters and gene bodies (Figure 3D; Additional file 1: Table S3B). DMCs in Cluster 3 were lowly methylated in NSCs and levels of DNAme increased following surgical repair at Day1 and Wk1 (Figure 3D).

To better understand the functional implications for the patterns of DNAme we observed, we performed GO and Kyoto Encyclopedia of Genes and Genomes (KEGG) enrichment analysis on the genes associated with identified DMC clusters. [22] Interestingly, we found DMCs in Cluster 3, which start out lowly methylated and gain methylation, were associated with genes that were enriched for GO (BP) terms associated with cytokine production (Figure S2A; Additional file 1: Table S3C). Genes associated with DMCs within promoters in Cluster 3 were not enriched for any KEGG pathways (Figure S2B; Additional file 1: Table S3D). In contrast, DMCs in Cluster 1, which are hypomethylated at post-surgical timepoints, were associated with genes that are enriched for GO (BPs) such as epithelial cell differentiation and regulation of cell migration (Figure S2C; Additional file 1: Table S3E). We found hypermethylated DMCs, found in Cluster 1 and Cluster 2, occur in genes involved in pathways that have been implicated in esophageal regeneration in previous studies. Specifically, genes associated with DMCs in Cluster 2 were enriched for KEGG pathways including vascular endothelial growth factor (VEGF), Ras, and PI3K-Akt (Figure S2B and S2D; Additional file 1: Table S3D and Table S3F). [23–25]

Next, to investigate whether methylation patterns were indicative of changes in gene regulatory elements, we determined whether DMC locations were enriched for certain classes of transcription factor binding sites (TFBS). We performed TFBS motif enrichment analysis in our DMCs using Hypergeometric Optimization of Motif EnRichment (HOMER). [26] We found Cluster 1 and Cluster 2 were enriched for several members of the basic helix-loop-helix (bHLH) family of transcription factors (TF) which have been implicated in cell lineage determination and differentiation (Figure S2E; Additional file 1: Table S3G). [27,28] DMCs in Cluster 3 were enriched for motifs associated with the ETS Homologous Factor (EHF) which targets genes that characterize epithelial-specific expression patterns, and E26 transformation-specific (ETS) TF family such as E74 Like ETS Transcription Factor 4 (Elf4) and ETS1 which have been implicated in cell proliferation, apoptosis, morphogenesis, and mesenchymal–epithelial interactions, especially during development (Figure S2E; Additional file 1: Table S3G). [29–31]

2.4 Hypomethylation occurs at CpG sites found in promoters of genes associated with immune activation.

To investigate which genes are targeted by DNA hypomethylation, which is a known regulatory mechanism for transcriptional expression, we first identified and characterized shared and unique HypoDMCs between timepoint comparisons (Figure 4A). To gain insight into the biological processes regulated through DNAme changes during esophageal

regeneration, we focused our analyses on HypoDMCs that were unique to each timepoint comparison. We identified 1,396 HypoDMCs unique to “NSC→Day1” (Figure 4A, orange shaded region), of which, 53% were found in gene bodies and 12% were found in promoters (Figure 4A and 4B; Additional file 1: Table S4A). We identified 6,898 HypoDMCs unique to “NSC→Wk1” (violet shaded region), of which, 55% were found in gene bodies and 12% were found in promoters (Figure 4A and 4B; Additional file 1: Table S4A). For unique HypoDMCs occurring within promoters, GO enrichment analysis of associated genes revealed a strong enrichment in BPs involved in immune activation and inflammation (Figure 4C, Additional file 1: Table S4B). Specifically, for the genes associated with unique NSC→Day1 HypoDMCs within promoters, we observed enrichment of BPs associated with NK T-cell activation and Interleukin-17 production, while genes associated with unique NSC→Wk1 HypoDMCs within promoters were enriched for leukocyte migration (Figure 4C, Additional file 1: Table S4B). To further identify signaling pathways that could be regulated by DNA hypomethylation within promoters, we performed pathway enrichment analysis on associated genes using Protein Analysis Through Evolutionary Relationships (PANTHER) Pathway. [32] This analysis could identify novel pathways involved in esophageal tissue regeneration. The genes associated with unique NSC→Wk1 HypoDMCs within promoters were enriched for PANTHER pathways involved in T-cell activation, angiogenesis, and Wnt signaling (Figure 4D; Additional file 1: Table S4C).

As DNAme occurring within the gene body has also been shown to modulate gene expression, we performed enrichment analysis for unique HypoDMCs that fall within the gene body. [33,34] GO enrichment analysis of genes associated with unique NSC→Day1 HypoDMCs within gene bodies revealed low enrichment for BPs including cholesterol homeostasis and lipid homeostasis (Figure 4E, Additional file 1: Table S4D). In contrast, the genes that were unique to NSC→Wk1 HypoDMCs within gene bodies were associated with cell morphogenesis (Figure 4E, Additional file 1: Table S4D). Genes associated with unique NSC→Wk1 HypoDMCs occurring in gene bodies were enriched for PANTHER pathways such as epidermal growth factor (EGF) and platelet-derived growth factor (PDGF) which are important signaling pathways involved in tissue regeneration and wound healing processes (Figure 4F, Additional file 1: Table S4E). [35–37] Notably, unique NSC→Day1 HypoDMCs within promoters and within gene bodies were not significantly enriched for any PANTHER pathways, which may be attributable to the smaller total number of unique NSC→Day1 HypoDMCs. Interestingly, we found NSC→Wk1 HypoDMCs occur in the promoter of the gene encoding DNMT3A, which conducts de novo methylation and interacts with histone methyltransferases to regulate transcriptional activity (Additional file 1: Table S4B). Both functions are critical for cell fate transitions and may contribute to cell proliferation and regeneration during wound healing processes. [38]

Next, we sought to determine how changes in DNA methylation could impact the binding of specific regulatory factors. We identified binding motifs enriched in unique HypoDMCs using HOMER. Unique HypoDMCs were enriched for binding motifs associated with regulatory factors involved in immune activation and inflammation such as interferon regulatory factors (Irf, Irf8), CCAAT enhancer-binding protein (Cebp), Elf4, and PU.1. [39,40] Motifs of RUNX TF family members, which have been shown to activate PI3K-Akt

pathways, were also enriched at HypoDMCs (Figure 4G, Additional file 1: Table S4F). [41,42]

2.5 Hypermethylation in post-surgical repair timepoints targets biological processes involved in PI3K-Akt signaling.

We identified 5,256 HyperDMCs unique to "NSC→Day1" (Figure 5A, orange shaded region), of which, 46% were found in gene bodies and 10% were found in promoters (Figure 5A and 5B; Additional file 1: Table S5A). We identified 21,954 HyperDMCs unique to "NSC→Wk1" (violet shaded region), of which, 55% were found in gene bodies and 10 % were found in promoters (Figure 5A and 5B; Additional file 1: Table S5A). GO enrichment analysis revealed that unique NSC→Day1 HyperDMCs occur within promoters of genes involved in receptor protein tyrosine kinase signaling and growth (Figure 5C, Additional file 1: Table S5B), while unique NSC→Wk1 HyperDMCs occur in genes involved in lipid oxidation and angiogenesis (Figure 5C, Additional file 1: Table S5B). PANTHER Pathway enrichment analysis revealed that unique NSC→Day1 HyperDMCs occur in promoters of genes involved in the VEGF signaling which is the major regulator of angiogenesis. [43] Unique NSC→Wk1 HyperDMCs occur in promoters of genes involved in muscarinic acetylcholine receptors 1 and 3 signaling (Figure 5D, Additional file 1: Table S5C).

We focused on hypermethylation that occurs at CpG sites within gene bodies, which has been shown to upregulate gene expression, for unique NSC→Day1 and NSC→Wk1 HyperDMCs. [34,44] Interestingly, both unique NSC→Day1 and NSC→Wk1 HyperDMCs occur within the gene bodies of genes involved in developmental BPs such as cell morphogenesis and tube development (Figure 5E, Additional file 1: Table S5D). This observation may suggest development BPs are upregulated in regenerating esophageal tissues following surgical injury. Most notably, PANTHER Pathway enrichment analysis revealed that unique NSC→Day1 and NSC→Wk1 HyperDMCs occur within gene bodies of genes involved in signaling pathways that have been previously implicated in tissue regeneration such as EGF, PDGF and Ras. [45,25,23] Ras activates PI3K-Akt signaling, which we previously showed was involved in neotissue formation following surgical repair with BLSF grafts (Figure 5F, Additional file 1: Table S5E). [8,46] P13K has also been shown to mediate PDGF and VEGF signaling. [47,24]

Hypermethylation of CpG sites can decrease the accessibility of TF binding to regulatory regions and can modulate the expression of genes and their downstream targets. [48,49] Motif analysis on unique HyperDMCs revealed an enrichment for motifs associated with the Forkhead (FOX) TF family (Foxa1, Foxo3, Foxm1, and Foxa2). The observed enrichment was more significant for NSC→Wk1 HyperDMCs than NSC→Day1 HyperDMCs (Figure 5G, Additional file 1: Table S5F). The Forkhead TF family has been shown to activate PI3K-Akt signaling which induces the transcription of genes that promote cell survival and suppress apoptotic responses. [50,51]

2.6 Putative enhancers lifted over from the human genome show dynamic methylation during esophageal regeneration

Given that we observe protein expression changes that correlate with DNAme changes at proximal regulatory elements (promoters and gene bodies), we also aimed to characterize differential methylation across distal regulatory elements. Due to the lack of annotations available for regulatory genomic features in the rat genome, we used the UCSC liftOver tool to lift human genome annotations to the rat genome to analyze differential methylation across conserved distal regulatory regions (Figure 6A). [52] First, we investigated the DNAme dynamics of CpGs that occur within conserved esophagus enhancer regions. Human esophagus gene-enhancer interaction networks were obtained from EnhancerAtlas 2.0 and lifted over to the rat genome with a 91% liftOver conversion rate (Additional file 1: Table S6A). [52] We found that the majority of the lifted esophagus enhancers resided within 100 kb of their associated gene's transcription start site (TSS) in the rat genome (Figure S3A). To obtain regional resolution of DNAme dynamics, we determined the average methylation levels for CpGs found across lifted esophagus enhancer regions. Lifted enhancers were considered to be differentially methylated if the average methylation level assigned to the lifted enhancer between the NSC condition and at each surgical timepoint exhibited a difference of at least 20%. Global analysis revealed CpGs that occur across lifted esophagus enhancers were hypermethylated at Day1 and Wk1 compared to NSC (Figure 6B; Additional file 1: Table S6B). We then focused on characterizing the methylation dynamics across conserved esophagus enhancers that were associated with genes, which we refer to as gene-enhancer pairs, that were also previously identified as DEPs during esophageal regeneration.[8] We found a comparable number of gene-enhancer pairs associated with genes encoding upregulated and downregulated DEPs in the NSC→Day1 comparison, while there were more gene-enhancer pairs associated with genes encoding upregulated DEPs compared to downregulated DEPs in the NSC→Wk1 comparison (Figure S6B). We determined the likelihood that differentially methylated lifted esophagus enhancers were associated with genes that encode DEPs using a logarithmic odds ratio (logOR) analysis (see Experimental Section). We analyzed the differentially methylated lifted gene-enhancer pairs and DEP directional expression for each timepoint comparison which revealed that hypomethylated gene-enhancer pairs were more strongly associated with DEPs that were upregulated at both timepoint comparisons (Figure 6C; Additional file 1: Table S6C). Our results suggest that the likelihood of hypermethylated lifted esophagus enhancers was positively associated with downregulated DEPs and negatively associated with upregulated DEPs at both timepoint comparisons (Figure 6C; Additional file 1: Table S6C). Similarly, we found a subtle association between hypomethylated lifted esophagus enhancers which were positively associated with upregulated DEPs and negatively associated with downregulated DEPs (Figure 6C; Additional file 1: Table S6C).

In our study, we showed that NSC→Day1 HypoDMCs were associated with genes involved in immune activation and this finding is supported by previous work that found neutrophils and mononuclear cells infiltrate the surgical implant site 1-day after BLSF surgery.[8] Based on these observations, we also investigated the DNAme dynamics of CpGs that occur across conserved neutrophil enhancer regions. Human neutrophil gene-enhancer interaction regions for the cell line (HL-60) were obtained from EnhancerAtlas 2.0 and lifted over

to the rat genome with a 91% liftOver conversion rate (Additional file 1: Table S6D).[52] Similar to the lifted esophagus enhancers, we characterized the average methylation levels for CpGs across lifted neutrophil gene-enhancer pairs and used a 20% methylation difference threshold to determine differentially methylated neutrophil gene-enhancer regions (Additional file 1: Table S6E). We found that the majority of lifted neutrophil enhancers resided within 100 kb of their associated gene's TSS in the rat genome (Figure S6C). Global analysis of methylation levels across lifted neutrophil enhancers showed that CpGs were hypermethylated at Day1 and Wk1 compared to NSC (Figure 6D). We focused on characterizing the methylation dynamics across conserved neutrophil gene-enhancer regions that were associated with genes that were previously identified as DEPs during esophageal regeneration.[8] We found a high number of gene-enhancer pairs associated with genes encoding upregulated compared to genes encoding downregulated DEPs for both timepoint comparison (Figure S6D). We performed a logOR analysis for differentially methylated lifted neutrophil gene-enhancer regions and DEP expression. Hypomethylated lifted neutrophil gene-enhancer regions showed the strongest association with upregulated DEPs for the NSC→Day1 comparison (Figure 6E; Additional file 1: Table S6F). In contrast, hypomethylated lifted neutrophil gene-enhancer regions were associated with both upregulated and downregulated DEPs for the NSC→Wk1 timepoint comparison (Figure 6E; Additional file 1: Table S6F). We found a slight association between hypermethylated lifted neutrophil gene-enhancer regions and upregulated DEPs and downregulated DEPs for the NSC→Wk1 (Figure 6E; Additional file 1: Table S6F). Our results suggest that the likelihood of hypomethylated lifted neutrophil enhancers in the NSC→Wk1 was positively associated with upregulated DEPs and was negatively associated with upregulated DEPs, while hypermethylated lifted neutrophil enhancers likelihood was negatively associated with upregulated DEPs and positively associated with downregulated DEPs (Figure 6E; Additional file 1: Table S6F). The implications of methylation dynamics of lifted neutrophil enhancers in the NSC→Day1 comparison was less clear but may reflect changes in cell populations found at the implant site, specifically infiltrating neutrophils after surgical repair.

3 Discussion

The application of bioengineered biomaterials in graft implants has therapeutic potential to improve the treatment and prognosis of patients with esophagus defects and other gastroenterological diseases.[6,7] Several pathways have been implicated in epithelial esophageal regeneration following surgical repair with acellular grafts previously in rats; however, the role of DNA methylation in tissue regeneration are not well understood.[7,8] In this report, we characterized changes in CpG methylation with RRBS in rat esophageal tissues following onlay esophagoplasty with BLSF grafts and during neoepithelial formation. Our findings indicate global hypermethylation occurs after surgery with acellular grafts at Day1 and Wk1 which correspond to post-surgical timepoints associated with neotissue formation (Figure 1).

Interestingly, while the majority of DMCs were hypermethylated in post-surgical timepoint samples, we found hypomethylated DMCs occur in promoters and the gene bodies of genes that are involved in immune activation and inflammation. We postulate that this

subset of hypomethylated DMCs may reflect changes in the cell populations present in the surgical implant site. Histological and proteomics findings from previous work found that inflammatory cells including neutrophils infiltrate surgical wounds sites one day after esophageal reconstruction.[8] Our results showed that hypomethylation occurs in CpGs of genes involved in immune activation after surgery. It is unclear whether the hypomethylated DMCs we identified reflect a new population of infiltrating immune cells or changes in DNAme levels of other cell types at the surgical implant site. Future studies using single-cell techniques can help identify cell-type specific epigenetic signatures in esophageal tissues during regeneration.[53,54]

Surprisingly, we found that site-specific hypermethylation appears to target several pathways which have been implicated in tissue regeneration in previous studies.[8] Specifically, it has been shown that epithelial esophageal regeneration is mediated, in part, through pro-survival stimuli and the inhibition of apoptotic pathways such as caspase and Baculoviral IAP Repeat Containing 3 (Birc3).[8] Our results showed that CpG hypermethylation occurs in promoters and gene bodies of genes involved in cytokine pathways which regulate cell growth and apoptotic signaling such as VEGF, PDGF and EGF receptor signaling (Figure 5C and 5D).[43] It has been demonstrated that promoter hypermethylation is important for repressing gene transcription, while gene body hypermethylation can upregulate gene expression.[55] Our findings provide evidence that epigenetic mechanisms, specifically promoter hypermethylation, may contribute to the inhibition of apoptotic signaling during regeneration. Additionally, we found several motifs in the Forkhead TF family which target genes that promote cell survival and suppress apoptotic signaling were enriched for HyperDMCs (Figure 5G).[50] Additional studies are required to assess how hypermethylation of Forkhead binding motifs affects transcription factor binding and gene regulation.

Whether the DNAme dynamics we observed here reflect a transient signaling response induced by surgical injury or changes to the cell populations found in the regenerating tissues is not clear. While further gene expression analyses, protein-DNA binding experiments, and gene-enhancer interaction network studies are necessary to elucidate how these pathways and their molecular components are precisely affected by changing DNAme dynamics, our work offers novel insight into potential epigenetic mechanisms that may be involved in esophageal regeneration, thereby identifying promising potential therapeutic targets that could be modulated to improve the regeneration process.

4 Experimental Section

Onlay rat esophagoplasty model

All in vivo procedures and animal husbandry were carried out pursuant to National Institutes of Health guide for the use of laboratory animals under the protocol number AUP-19–153 approved by the Animal Care and Use Committee of the University of California, Irvine. Adult male Sprague-Dawley rats (Charles River Laboratories, San Diego, CA) weighing 260–300 grams were randomized into the 3 groups according to implantation period including nonsurgical controls (NSC) (n=8), Day1 post-op (n=8), and Wk1 post-op (n=8). Day1 and Wk1 groups were subjected to onlay esophagoplasty with BLSF

grafts using published protocols, [56] as described below. Prior to surgical reconstruction, animals were single housed in wire cages and maintained on a nutritionally balanced liquid diet formulation (TestDiet, Richmond, IN mixed with PediaSure, Abbott Laboratories, Columbus, OH) for Day1 prior to surgery and continued for 3 days post-operatively. In addition, rats were also given to free access water during the entire study period. General anesthesia was induced and maintained by 2–4% isoflurane inhalation. Abdominal fur was then clipped, and the skin was sterilized with betadine and 70% ethanol. The surgical area was covered by sterile drapes. The intra-abdominal portion of the lower esophagus was approached by a vertical midline abdominal incision. The esophagus was then pulled to the skin level using two vessel loops and a full thickness 7×3 mm elliptical defect was created on the anterior esophageal wall. The defect was repaired with an equal sized BLSF graft via anastomosis with the surrounding host tissue using absorbable 7–0 polyglactin running sutures. Four 7–0 nonabsorbable polypropylene sutures were positioned at the proximal/distal and lateral edges of the implanted matrix in order to identify the original scaffold margins. The scaffold was then covered with an omental patch to minimize any potential leakage from the suture line and the esophagus was placed back into the abdomen and tissue layers were sutured closed. Post-operative pain control was managed with 0.5% bupivacaine diluted 1:1 with saline as well as Buprenorphine SR (1.2 mg/kg, subcutaneously) and fluxine meglumine (2.5 mg/kg; subcutaneously). Animals received enrofloxacin (5mg/kg; 3 days post-operatively, subcutaneously) for mitigation of potential bacterial infection. All rats were transferred from liquid diet to standard rat chow 3 days after surgery and were euthanized by carbon dioxide asphyxiation at experimental timepoints. Following animal harvest, esophageal tissues from each group were equally segregated for either epigenetic or histological/immunohistochemical analyses (n=4 per group for each assay). For epigenetic studies, biopsy punches were utilized to acquire host esophageal tissues surrounding 2 mm of the original defect circumference at Day1 post-op, while neotissues at Wk1 post-op were isolated from the initial graft area. Full thickness esophageal specimens were harvested in parallel from NSC for baseline epigenetic evaluations.

Histological and immunohistochemical (IHC) analyses

Reconstructed esophageal segments (N=4 per timepoint) as well as nonsurgical control (NSC) specimens (N=4) were fixed in 10% formalin for 12 hours, dehydrated in graded alcohols, and paraffin embedded. Tissue sections (5 μm) were stained with Masson's trichrome to reveal global tissue architecture using standard histological protocols. Masson's trichrome staining and immunohistochemical (IHC) analyses were performed on four biological replicates in each condition: non-surgical controls (NSCs), Day1, and Wk1 (n=4 for each condition). IHC evaluations were performed on tissue sections following antigen retrieval (10 mM sodium citrate buffer, pH 6.0) and incubation in phosphate-buffered saline with 0.3% Triton X-100, 5% fetal bovine serum, and 1% bovine serum albumin for 1 hour at room temperature. Sections were then stained with primary antibodies including anti-DNA methyltransferase (DNMT)1 (cat. # 24206–1-AP, 1:200 dilution, Proteintech, Rosemont, IL), anti-DNMT3A (cat. #GTX129125, 1:200 dilution, GeneTex, Irvine, CA), anti-DNMT3B (cat. # PA1–884, 1:200 dilution, Invitrogen, Waltham, MA), anti-cytokeratin (CK)5 [cat. # ab53121, 1:200 dilution, Abcam], and anti-filaggrin (FG) (cat. #sc-80609, 1:200 dilution, Santa Cruz Biotechnology). For DNMT1, 3A, and 3B detection, specimens

were then incubated with species-matched horseradish peroxidase (HRP)-conjugated secondary antibodies in combination with hematoxylin counterstain. For CK5 and filaggrin detection, samples were probed with species-matched Alexa Fluor 488 and 647-conjugated secondary antibodies (Thermo Fisher Scientific) and nuclear counterstain was carried out with 4′, 6-diamidino-2-phenyllindole (DAPI). An Axioplan-2 microscope (Carl Zeiss MicroImaging, Thornwood, NY) was deployed for sample visualization and representative fields were acquired with Axiovision software (version 4.8).

RRBS Library preparation

10mg of tissue each was collected for DNA isolation using Qiagen DNeasy Blood & Tissue kit (Qiagen, Hilden, Germany). 4.5ug of genomic DNA was digested with MspI overnight. The digested products were size-selected using AMPure XP beads to remove anything above 300bp or small fragment retention. 100ng size-selected DNA was bisulfite-converted using EZ DNA Methylation-Gold Kit (Zymo Research, Irvine, CA). The eluted DNA was performed immediately using the Accel-NGS Methyl-seq DNA library kit (Swift Biosciences, Ann Arbor, MI) according to the manufacturer's instructions. Final libraries were generated from 9–14 PCR cycles. PCR products were cleaned up using the SPRIselect beads (Beckman Coulter, Orange, CA) to remove the primer dimers. Libraries were confirmed by an Agilent Bioanalyzer, and the yields were quantified by KAPA qPCR. Sequencing was performed at the UCI Genomics High Throughput Facility. 100bp paired-end reads were sequenced by Illumina Nova-seq 6000 sequencing system.

RRBS data processing and detection of DMCs

Adaptor and low-quality RRBS reads in FASTQ format were trimmed and filtered using Trim Galore (version 0.6.6) with the following parameters: "--paired --clip_r1 10 --clip_r2 15 --three_prime_clip_r1 10 --three_prime_clip_r2 10 --fastqc". Reads were aligned to the rat genome (mRatBN7.2/rn7, data: 2020/11/10) with Bismark (version 0.23.0) [57]. On average, 22.8 million trimmed reads per sample were aligned to rat genome (mRatBN7.2/rn7, release 105, Ensembl). As a quality control measure, the RRBS data analysis as performed on biological replicates that had a mapping efficiency value ≥70%. CpG sites were called using the "bismark_methylation_extractor" function (--comprehensive option) in Bismark. Differential methylated cytosines (DMCs) were called with methylKit (version 1.14.2) for CpGs with a minimum of 5 counts.[58]

Genomic feature annotations

The methylation percentages for genomic regions, gene bodies, promoters, 5′-UTRs, exons, introns and 3′-UTRs were found using BEDTools' intersect function to finding the overlapping CpGs (≥5x coverage) in the sample BED files and genomic tracks from UCSC genome table browser (BEDTools version 2.25.0). Intergenic features were acquired by finding regions outside of gene bodies using BEDTools' complement function and the size of each chromosomes in the rat genome (rn7) which was obtained by downloading the rn7.chrom.sizes.txt file from NCBI.[59,60] Genomic promoter features were defined as 2kb upstream and 500bp downstream of gene transcription start sites (TSS) acquired from UCSC genome table browser. Gene body features were defined as 500bp downstream of TSS from

UCSC genome table browser to prevent overlap between the promoter track and gene body track.

Identification of gene network and ontologies from DMC-associated gene lists

The list of genes associated with DMCs were obtained by intersecting locations of CpGs with locations of annotated genes in the rat genome assembly (mRatBN7.2) obtained from NCBI Rattus norvegicus Annotation Release 108 (Assembly accession: GCF_015227675.2). The enrichment analysis was performed on the genes associated with DMCs within promoters and within gene bodies for Gene Ontology (GO) Biological Processes (BP), Protein Analysis Through Evolutionary Relationships (PANTHER) Pathway, and Kyoto Encyclopedia of Genes and Genomes (KEGG) enriched pathways using ShinyGO (version 0.75).[22,32,61,62] Enriched GO (BP) and pathways were filtered using a false discovery rate (calculated according to the Benjamini & Hochberg method)≤ 0.05.[63]

Determining differentially methylated transcription factor binding sites (TFBS)

DMC files, in BED format, were inputted into Hypergeometric Optimization of Motif EnRichment (HOMER) software (Version 4.11) to identify enrichment of known TFBS motifs, reposited within the software's vertebrae database.[26] BED files were converted to Rnor_6.0 genome assembly version with UCSC's liftOver tool. Analyses were performed with the list of CpGs (5x coverage) present in at least 3 replicates per experimental condition as background and the motif size parameter set to 200bp. TFBS motif results were finally filtered for p-value≤ 0.01.

LiftOver human enhancer tracks

Human enhancer-gene interaction networks annotated in hg19 for esophagus whole cell and the neutrophil-like cell line (HL-60) were obtained from EnhancerAtlas 2.0.[52] The downloaded files were processed with Python 3.0 to create BED files that include the chromosome number, start and end coordinates of the enhancer region, strandedness, and the associated gene names. The UCSC liftOver tool was used to lift over BED files from the human genome to the rat genome. Minimum ratio of bases that must remap was set at 0.1. BED files for hg19 enhancer tracks were first lifted over to the hg38 genome (100% liftOver conversion rate) and then lifted over to the rat genome (rn7) (91% liftOver conversion rate) since the liftOver tool does not allow for a direct conversion from hg19 to rn7.

Determining differentially methylated lifted enhancers

The BED files containing our filtered set of CpGs (≥5x coverage found in ≥3 samples in each condition, n=514,813) for each timepoint were intersected with lifted enhancer BED files obtained from EnhancerAtlas 2.0 using BEDTools (version 2.25.0). We calculated the average methylation values for CpGs for each lifted enhancer. Differentially methylated enhancers were identified using a 20% threshold value for the methylation difference between each surgical timepoint compared to the NSC (i.e., NSC→Day1 and NSC→Wk1). We filtered the lifted unique gene-enhancer pairs for genes that were previously identified as DEPs during esophageal regeneration based on data from Gundogdu et al. Sci Reports. 2021.[8] Logarithmic odds ratio (logOR) analyses were performed to determine the

significance of differentially methylated gene-enhancers pairs with genes encoding DEPs. Our confusion matrices were configured to consider hypomethylated/hypermethylated or not lifted enhancers and upregulated/downregulated or not DEPs. Fisher's exact test was used to determine the significance of odds ratios using R (version 4.0.5).

Statistical Analysis

All statistical tests were performed with R (version 4.0.5). To ensure high-quality reads were used in the analysis, only RRBS samples with an alignment efficiency of 70% or greater were used in downstream data analysis which resulted in the following number of biological replicates: NSC (n=4), Day1 (n=5), and Wk1 (n=4). Significance values were calculated using the Wilcoxon rank-sum test in R (version 4.0.5) because the data did not follow a Gaussian distribution. The *p*-values were listed in each figures and *ns* indicates a *p*-value >0.05. Euclidean hierarchical clustering was performed on CpGs with >5x coverage that were captured in all samples: NSC (n=4), Day1 (n=5), and Wk1 (n=4) (n=3,494 CpGs). The hierarchical clustering was performed with pHeatmap package (version 1.0.12) using the Ward's minimum variance method (Ward.D2) clustering method in RStudio (version 4.0.5). DMC statistical analysis was performed on CpGs with >5x coverage that were found in a minimum of three biological replicates in each condition and were present across all conditions (n=514,813 CpGs). DMCs were determined by comparing in the mean differences in methylated calls for a particular cytosine between the non-surgical controls and post-op timepoint samples using a threshold value of q-value <0.01 and meth.diff value >20% using the R package methylKit (Version 1.16.0). The DEP data was obtained from Gundogdu et al. Sci Reports. 2021 which identified DEPs from proteomic analysis of regenerating rat esophageal tissues following repair with acellular grafts using a threshold value of >2-fold (log2ratio >1 or <−1) between the NSC controls and post-surgical timepoints (1 day, 1 week, 1 month, 2 months post-op) (N= 4 for experimental condition).[8]

Supplementary Material

Refer to Web version on PubMed Central for supplementary material.

ACKNOWLEDGEMENTS

This work was supported, in large part, by a National Institutes of Health (NIH) New Innovator Award (DP2) Grant DP2CA250382-01, an NIH National Institute of Biomedical Imaging and Bioengineering (NIBIB) Grant R21EB027840-01, a National Science Foundation (NSF) grant (DMS1763272), and a grant from the Simons Foundation (594598) to T.L.D. and NIH grant R01-DK119240 to J.R.M. This work was also supported by a grant from the California Institute for Regenerative Medicine (Award Number EDUC4-12822) awarded to A.T. and the Stanley Behrens Fellows in Medicine Award to L.U.

Data Availability Statement

Raw data for all figures are available in the Supplementary Information Source Data file. The RRBS data are freely available under the National Center for Biotechnology Information Gene Expression Omnibus (GEO) accession number is GSE203028.

REFERENCES

1. Raboei E, Luoma R, Colon Patch Esophagoplasty: An Alternative to Total Esophagus Replacement? Eur J Pediatr Surg 18, 230–232 (2008). [PubMed: 18629764]
2. Benazzo M, Spasiano R, Bertino G, Occhini A, Gatti P, Sternocleidomastoid Muscle Flap in Esophageal Perforation Repair After Cervical Spine Surgery: Concepts, Techniques, and Personal Experience. Journal of Spinal Disorders & Techniques 21, 597–605 (2008). [PubMed: 19057255]
3. Ki SH, Choi JH, Sim SH, Reconstructive Trends in Post-Ablation Patients with Esophagus and Hypopharynx Defect. Arch Craniofac Surg 16, 105 (2015). [PubMed: 28913234]
4. Lin Y-C, Hsiao J-R, Lee Y-C, Patch esophagoplasty with a free proximal lateral leg flap for focal stricture of the cervical esophagus: A case report: Patch Esophagoplasty with Proximal Lateral Leg Flap. Microsurgery 37, 426–430 (2017). [PubMed: 26800296]
5. Genden EM, Jacobson AS, The role of the anterolateral thigh flap for pharyngoesophageal reconstruction. Arch Otolaryngol Head Neck Surg 131, 796–799 (2005). [PubMed: 16172358]
6. Maghsoudlou P, Eaton S, De Coppi P, Tissue engineering of the esophagus. Semin Pediatr Surg 23, 127–134 (2014). [PubMed: 24994526]
7. Algarrahi K, Franck D, Ghezzi CE, Cristofaro V, Yang X, Sullivan MP, Chung YG, Affas S, Jennings R, Kaplan DL, Estrada CR, Mauney JR, Acellular bi-layer silk fibroin scaffolds support functional tissue regeneration in a rat model of onlay esophagoplasty. Biomaterials 53, 149–159 (2015). [PubMed: 25890715]
8. Gundogdu G, Tosun M, Morhardt D, Gheinani AH, Algarrahi K, Yang X, Costa K, Alegria CG, Adam RM, Yang W, Mauney JR, Molecular mechanisms of esophageal epithelial regeneration following repair of surgical defects with acellular silk fibroin grafts. Sci Rep 11, 7086 (2021). [PubMed: 33782465]
9. Moore LD, Le T, Fan G, DNA Methylation and Its Basic Function. Neuropsychopharmacol 38, 23–38 (2013).
10. Wang W, Xie Y, Zhou Z, Qin Z, Wu J, He J, PIK3CA hypomethylation plays a key role in activation of the PI3K/AKT pathway in esophageal cancer in Chinese patients. Acta Pharmacol Sin 34, 1560–1567 (2013). [PubMed: 24241346]
11. Ogunwobi OO, Puszyk W, Dong H-J, Liu C, Epigenetic upregulation of HGF and c-Met drives metastasis in hepatocellular carcinoma. PLoS One 8, e63765 (2013).
12. Jin W, Lee J-J, Kim MS, Son BH, Cho YK, Kim H-P, DNA methylation-dependent regulation of TrkA, TrkB, and TrkC genes in human hepatocellular carcinoma. Biochem Biophys Res Commun 406, 89–95 (2011). [PubMed: 21295543]
13. Chen Y, Fan Z, Wang X, Mo M, Zeng SB, Xu R-H, Wang X, Wu Y, PI3K/Akt signaling pathway is essential for de novo hair follicle regeneration. Stem Cell Res Ther 11, 144 (2020).
14. Chmielowiec J, Borowiak M, Morkel M, Stradal T, Munz B, Werner S, Wehland J, Birchmeier C, Birchmeier W, c-Met is essential for wound healing in the skin. Journal of Cell Biology 177, 151–162 (2007). [PubMed: 17403932]
15. Zheng M-G, Sui W-Y, He Z-D, Liu Y, Huang Y-L, Mu S-H, Xu X-Z, Zhang J-S, Qu J-L, Zhang J, Wang D, TrkA regulates the regenerative capacity of bone marrow stromal stem cells in nerve grafts. Neural Regen Res 14, 1765 (2019). [PubMed: 31169194]
16. Boison D, Masino SA, Lubin FD, Guo K, Lusardi T, Sanchez R, Ruskin DN, Ohm J, Geiger JD, Hur J, The impact of methodology on the reproducibility and rigor of DNA methylation data. Sci Rep 12, 380 (2022). [PubMed: 35013473]
17. Zhu M, Li W, Dong X, Yuan X, Midgley AC, Chang H, Wang Y, Wang H, Wang K, Ma PX, Wang H, Kong D, In vivo engineered extracellular matrix scaffolds with instructive niches for oriented tissue regeneration. Nat Commun 10, 4620 (2019). [PubMed: 31604958]
18. Ryckman C, Vandal K, Rouleau P, Talbot M, Tessier PA, Proinflammatory activities of S100: proteins S100A8, S100A9, and S100A8/A9 induce neutrophil chemotaxis and adhesion. J Immunol 170, 3233–3242 (2003). [PubMed: 12626582]
19. Pervushina O, Scheuerer B, Reiling N, Behnke L, Schröder J-M, Kasper B, Brandt E, Bulfone-Paus S, Petersen F, Platelet factor 4/CXCL4 induces phagocytosis and the generation of

reactive oxygen metabolites in mononuclear phagocytes independently of Gi protein activation or intracellular calcium transients. J Immunol 173, 2060–2067 (2004). [PubMed: 15265941]

20. Maurer A-M, Zhou B, Han ZC, Roles of platelet factor 4 in hematopoiesis and angiogenesis. Growth Factors 24, 242–252 (2006). [PubMed: 17381065]
21. Wu X, Yang SL, Yerle M, Zhu ZM, Wang HL, Wang H, Li K, Genomic organization, localization and polymorphism of porcine PSMB10, a gene encoding the third beta-type proteasome subunit of 26S proteasome complex. J Anim Breed Genet 123, 331–336 (2006). [PubMed: 16965406]
22. Kanehisa M, Goto S, KEGG: kyoto encyclopedia of genes and genomes. Nucleic Acids Res 28, 27–30 (2000). [PubMed: 10592173]
23. Gross SM, Rotwein P, Mapping growth-factor-modulated Akt signaling dynamics. J Cell Sci 129, 2052–2063 (2016). [PubMed: 27044757]
24. Wang D, Huang HJ, Kazlauskas A, Cavenee WK, Induction of vascular endothelial growth factor expression in endothelial cells by platelet-derived growth factor through the activation of phosphatidylinositol 3-kinase. Cancer Res 59, 1464–1472 (1999). [PubMed: 10197615]
25. Ross R, Bowen-Pope DF, Raines EW, Platelet-derived growth factor: its potential roles in wound healing, atherosclerosis, neoplasia, and growth and development. Ciba Found Symp 116, 98–112 (1985). [PubMed: 3000710]
26. Heinz S, Benner C, Spann N, Bertolino E, Lin YC, Laslo P, Cheng JX, Murre C, Singh H, Glass CK, Simple combinations of lineage-determining transcription factors prime cis-regulatory elements required for macrophage and B cell identities. Mol Cell 38, 576–589 (2010). [PubMed: 20513432]
27. Martin JF, Li L, Olson EN, Repression of myogenin function by TGF-beta 1 is targeted at the basic helix-loop-helix motif and is independent of E2A products. J Biol Chem 267, 10956–10960 (1992). [PubMed: 1317849]
28. Hu JS, Olson EN, Kingston RE, HEB, a helix-loop-helix protein related to E2A and ITF2 that can modulate the DNA-binding ability of myogenic regulatory factors. Mol Cell Biol 12, 1031–1042 (1992). [PubMed: 1312219]
29. Kola I, Brookes S, Green AR, Garber R, Tymms M, Papas TS, Seth A, The Ets1 transcription factor is widely expressed during murine embryo development and is associated with mesodermal cells involved in morphogenetic processes such as organ formation. Proc Natl Acad Sci U S A 90, 7588–7592 (1993). [PubMed: 7689222]
30. Thompson CB, Wang CY, Ho IC, Bohjanen PR, Petryniak B, June CH, Miesfeldt S, Zhang L, Nabel GJ, Karpinski B, cis-acting sequences required for inducible interleukin-2 enhancer function bind a novel Ets-related protein, Elf-1. Mol Cell Biol 12, 1043–1053 (1992). [PubMed: 1545787]
31. Tugores A, Le J, Sorokina I, Snijders AJ, Duyao M, Reddy PS, Carlee L, Ronshaugen M, Mushegian A, Watanaskul T, Chu S, Buckler A, Emtage S, McCormick MK, The epithelium-specific ETS protein EHF/ESE-3 is a context-dependent transcriptional repressor downstream of MAPK signaling cascades. J Biol Chem 276, 20397–20406 (2001). [PubMed: 11259407]
32. Mi H, Muruganujan A, Casagrande JT, Thomas PD, Large-scale gene function analysis with the PANTHER classification system. Nat Protoc 8, 1551–1566 (2013). [PubMed: 23868073]
33. Mendizabal I, Zeng J, Keller TE, Yi SV, Body-hypomethylated human genes harbor extensive intragenic transcriptional activity and are prone to cancer-associated dysregulation. Nucleic Acids Res 45, 4390–4400 (2017). [PubMed: 28115635]
34. Yang X, Han H, De Carvalho DD, Lay FD, Jones PA, Liang G, Gene body methylation can alter gene expression and is a therapeutic target in cancer. Cancer Cell 26, 577–590 (2014). [PubMed: 25263941]
35. Laato M, Niinikoski J, Lebel L, Gerdin B, Stimulation of wound healing by epidermal growth factor. A dose-dependent effect. Ann Surg 203, 379–381 (1986). [PubMed: 3485960]
36. Buckley A, Davidson JM, Kamerath CD, Wolt TB, Woodward SC, Sustained release of epidermal growth factor accelerates wound repair. Proc Natl Acad Sci U S A 82, 7340–7344 (1985). [PubMed: 3877308]
37. Petroutsos G, Courty J, Guimaraes R, Pouliquen Y, Barritault D, Plouët J, Courtois Y, Comparison of the effects of EGF, pFGF and EDGF on corneal epithelium wound healing. Curr Eye Res 3, 593–598 (1984). [PubMed: 6609050]

38. Okano M, Bell DW, Haber DA, Li E, DNA methyltransferases Dnmt3a and Dnmt3b are essential for de novo methylation and mammalian development. Cell 99, 247–257 (1999). [PubMed: 10555141]
39. Marecki S, Riendeau CJ, Liang MD, Fenton MJ, PU.1 and multiple IFN regulatory factor proteins synergize to mediate transcriptional activation of the human IL-1 beta gene. J Immunol 166, 6829–6838 (2001). [PubMed: 11359842]
40. Yamada T, Park CS, Mamonkin M, Lacorazza HD, Transcription factor ELF4 controls the proliferation and homing of CD8+ T cells via the Krüppel-like factors KLF4 and KLF2. Nat Immunol 10, 618–626 (2009). [PubMed: 19412182]
41. Edwards H, Xie C, LaFiura KM, Dombkowski AA, Buck SA, Boerner JL, Taub JW, Matherly LH, Ge Y, RUNX1 regulates phosphoinositide 3-kinase/AKT pathway: role in chemotherapy sensitivity in acute megakaryocytic leukemia. Blood 114, 2744–2752 (2009). [PubMed: 19638627]
42. Fujita T, Azuma Y, Fukuyama R, Hattori Y, Yoshida C, Koida M, Ogita K, Komori T, Runx2 induces osteoblast and chondrocyte differentiation and enhances their migration by coupling with PI3K-Akt signaling. J Cell Biol 166, 85–95 (2004). [PubMed: 15226309]
43. Baatar D, Jones MK, Tsugawa K, Pai R, Moon WS, Koh GY, Kim I, Kitano S, Tarnawski AS, Esophageal ulceration triggers expression of hypoxia-inducible factor-1 alpha and activates vascular endothelial growth factor gene: implications for angiogenesis and ulcer healing. Am J Pathol 161, 1449–1457 (2002). [PubMed: 12368217]
44. Murrell A, Heeson S, Bowden L, Constância M, Dean W, Kelsey G, Reik W, An intragenic methylated region in the imprinted Igf2 gene augments transcription. EMBO Rep 2, 1101–1106 (2001). [PubMed: 11743023]
45. Tarnawski AS, Ahluwalia A, Molecular mechanisms of epithelial regeneration and neovascularization during healing of gastric and esophageal ulcers. Curr Med Chem 19, 16–27 (2012). [PubMed: 22300072]
46. Fang X, Yu S, Eder A, Mao M, Bast RC, Boyd D, Mills GB, Regulation of BAD phosphorylation at serine 112 by the Ras-mitogen-activated protein kinase pathway. Oncogene 18, 6635–6640 (1999). [PubMed: 10597268]
47. Chung J, Grammer TC, Lemon KP, Kazlauskas A, Blenis J, PDGF- and insulin-dependent pp70S6k activation mediated by phosphatidylinositol-3-OH kinase. Nature 370, 71–75 (1994). [PubMed: 8015612]
48. Luo X, Zhang T, Zhai Y, Wang F, Zhang S, Wang G, Effects of DNA Methylation on TFs in Human Embryonic Stem Cells. Front Genet 12, 639461 (2021).
49. Medvedeva YA, Khamis AM, Kulakovskiy IV, Ba-Alawi W, Bhuyan MSI, Kawaji H, Lassmann T, Harbers M, Forrest ARR, Bajic VB, FANTOM consortium, Effects of cytosine methylation on transcription factor binding sites. BMC Genomics 15, 119 (2014). [PubMed: 24669864]
50. Yano S, Tokumitsu H, Soderling TR, Calcium promotes cell survival through CaM-K kinase activation of the protein-kinase-B pathway. Nature 396, 584–587 (1998). [PubMed: 9859994]
51. Tullai JW, Schaffer ME, Mullenbrock S, Kasif S, Cooper GM, Identification of Transcription Factor Binding Sites Upstream of Human Genes Regulated by the Phosphatidylinositol 3-Kinase and MEK/ERK Signaling Pathways. Journal of Biological Chemistry 279, 20167–20177 (2004). [PubMed: 14769801]
52. Gao T, Qian J, EnhancerAtlas 2.0: an updated resource with enhancer annotation in 586 tissue/cell types across nine species. Nucleic Acids Research, gkz980 (2019).
53. Schmidt M, Maié T, Dahl E, Costa IG, Wagner W, Deconvolution of cellular subsets in human tissue based on targeted DNA methylation analysis at individual CpG sites. BMC Biol 18, 178 (2020). [PubMed: 33234153]
54. Stueve TR, Marconett CN, Zhou B, Borok Z, Laird-Offringa IA, The importance of detailed epigenomic profiling of different cell types within organs. Epigenomics 8, 817–829 (2016). [PubMed: 27305639]
55. Rauluseviciute I, Drabløs F, Rye MB, DNA hypermethylation associated with upregulated gene expression in prostate cancer demonstrates the diversity of epigenetic regulation. BMC Med Genomics 13, 6 (2020). [PubMed: 31914996]

56. Gundogdu G, Tosun M, Morhardt D, Gheinani AH, Algarrahi K, Yang X, Costa K, Alegria CG, Adam RM, Yang W, Mauney JR, Molecular mechanisms of esophageal epithelial regeneration following repair of surgical defects with acellular silk fibroin grafts. Sci Rep 11, 7086 (2021). [PubMed: 33782465]
57. Krueger F, Andrews SR, Bismark: a flexible aligner and methylation caller for Bisulfite-Seq applications. Bioinformatics 27, 1571–1572 (2011). [PubMed: 21493656]
58. Akalin A, Kormaksson M, Li S, Garrett-Bakelman FE, Figueroa ME, Melnick A, Mason CE, methylKit: a comprehensive R package for the analysis of genome-wide DNA methylation profiles. Genome Biol 13, R87 (2012). [PubMed: 23034086]
59. Gibbs RA, Weinstock GM, Metzker ML, Muzny DM, Sodergren EJ, Scherer S, Scott G, Steffen D, Worley KC, Burch PE, Okwuonu G, Hines S, Lewis L, DeRamo C, Delgado O, Dugan-Rocha S, Miner G, Morgan M, Hawes A, Gill R, null Celera RA Adams Holt, M. D., Amanatides PG, Baden-Tillson H, Barnstead M, Chin S, Evans CA, Ferriera S, Fosler C, Glodek A, Gu Z, Jennings D, Kraft CL, Nguyen T, Pfannkoch CM, Sitter C, Sutton GG, Venter JC, Woodage T, Smith D, Lee H-M, Gustafson E, Cahill P, Kana A, Doucette-Stamm L, Weinstock K, Fechtel K, Weiss RB, Dunn DM, Green ED, Blakesley RW, Bouffard GG, De Jong PJ, Osoegawa K, Zhu B, Marra M, Schein J, Bosdet I, Fjell C, Jones S, Krzywinski M, Mathewson C, Siddiqui A, Wye N, McPherson J, Zhao S, Fraser CM, Shetty J, Shatsman S, Geer K, Chen Y, Abramzon S, Nierman WC, Havlak PH, Chen R, Durbin KJ, Egan A, Ren Y, Song X-Z, Li B, Liu Y, Qin X, Cawley S, Worley KC, Cooney AJ, D'Souza LM, Martin K, Wu JQ, Gonzalez-Garay ML, Jackson AR, Kalafus KJ, McLeod MP, Milosavljevic A, Virk D, Volkov A, Wheeler DA, Zhang Z, Bailey JA, Eichler EE, Tuzun E, Birney E, Mongin E, Ureta-Vidal A, Woodwark C, Zdobnov E, Bork P, Suyama M, Torrents D, Alexandersson M, Trask BJ, Young JM, Huang H, Wang H, Xing H, Daniels S, Gietzen D, Schmidt J, Stevens K, Vitt U, Wingrove J, Camara F, Mar Albà M, Abril JF, Guigo R, Smit A, Dubchak I, Rubin EM, Couronne O, Poliakov A, Hübner N, Ganten D, Goesele C, Hummel O, Kreitler T, Lee Y-A, Monti J, Schulz H, Zimdahl H, Himmelbauer H, Lehrach H, Jacob HJ, Bromberg S, Gullings-Handley J, Jensen-Seaman MI, Kwitek AE, Lazar J, Pasko D, Tonellato PJ, Twigger S, Ponting CP, Duarte JM, Rice S, Goodstadt L, Beatson SA, Emes RD, Winter EE, Webber C, Brandt P, Nyakatura G, Adetobi M, Chiaromonte F, Elnitski L, Eswara P, Hardison RC, Hou M, Kolbe D, Makova K, Miller W, Nekrutenko A, Riemer C, Schwartz S, Taylor J, Yang S, Zhang Y, Lindpaintner K, Andrews TD, Caccamo M, Clamp M, Clarke L, Curwen V, Durbin R, Eyras E, Searle SM, Cooper GM, Batzoglou S, Brudno M, Sidow A, Stone EA, Venter JC, Payseur BA, Bourque G, López-Otín C, Puente XS, Chakrabarti K, Chatterji S, Dewey C, Pachter L, Bray N, Yap VB, Caspi A, Tesler G, Pevzner PA, Haussler D, Roskin KM, Baertsch R, Clawson H, Furey TS, Hinrichs AS, Karolchik D, Kent WJ, Rosenbloom KR, Trumbower H, Weirauch M, Cooper DN, Stenson PD, Ma B, Brent M, Arumugam M, Shteynberg D, Copley RR, Taylor MS, Riethman H, Mudunuri U, Peterson J, Guyer M, Felsenfeld A, Old S, Mockrin S, Collins F, Rat Genome Sequencing Project Consortium, Genome sequence of the Brown Norway rat yields insights into mammalian evolution. Nature 428, 493–521 (2004). [PubMed: 15057822]
60. Havlak P, Chen R, Durbin KJ, Egan A, Ren Y, Song X-Z, Weinstock GM, Gibbs RA, The Atlas genome assembly system. Genome Res 14, 721–732 (2004). [PubMed: 15060016]
61. Ge SX, Jung D, Yao R, ShinyGO: a graphical gene-set enrichment tool for animals and plants. Bioinformatics 36, 2628–2629 (2020). [PubMed: 31882993]
62. Ashburner M, Ball CA, Blake JA, Botstein D, Butler H, Cherry JM, Davis AP, Dolinski K, Dwight SS, Eppig JT, Harris MA, Hill DP, Issel-Tarver L, Kasarskis A, Lewis S, Matese JC, Richardson JE, Ringwald M, Rubin GM, Sherlock G, Gene Ontology: tool for the unification of biology. Nat Genet 25, 25–29 (2000). [PubMed: 10802651]
63. Benjamini Y, Hochberg Y, Controlling the False Discovery Rate: A Practical and Powerful Approach to Multiple Testing. Journal of the Royal Statistical Society. Series B (Methodological) 57, 289–300 (1995).

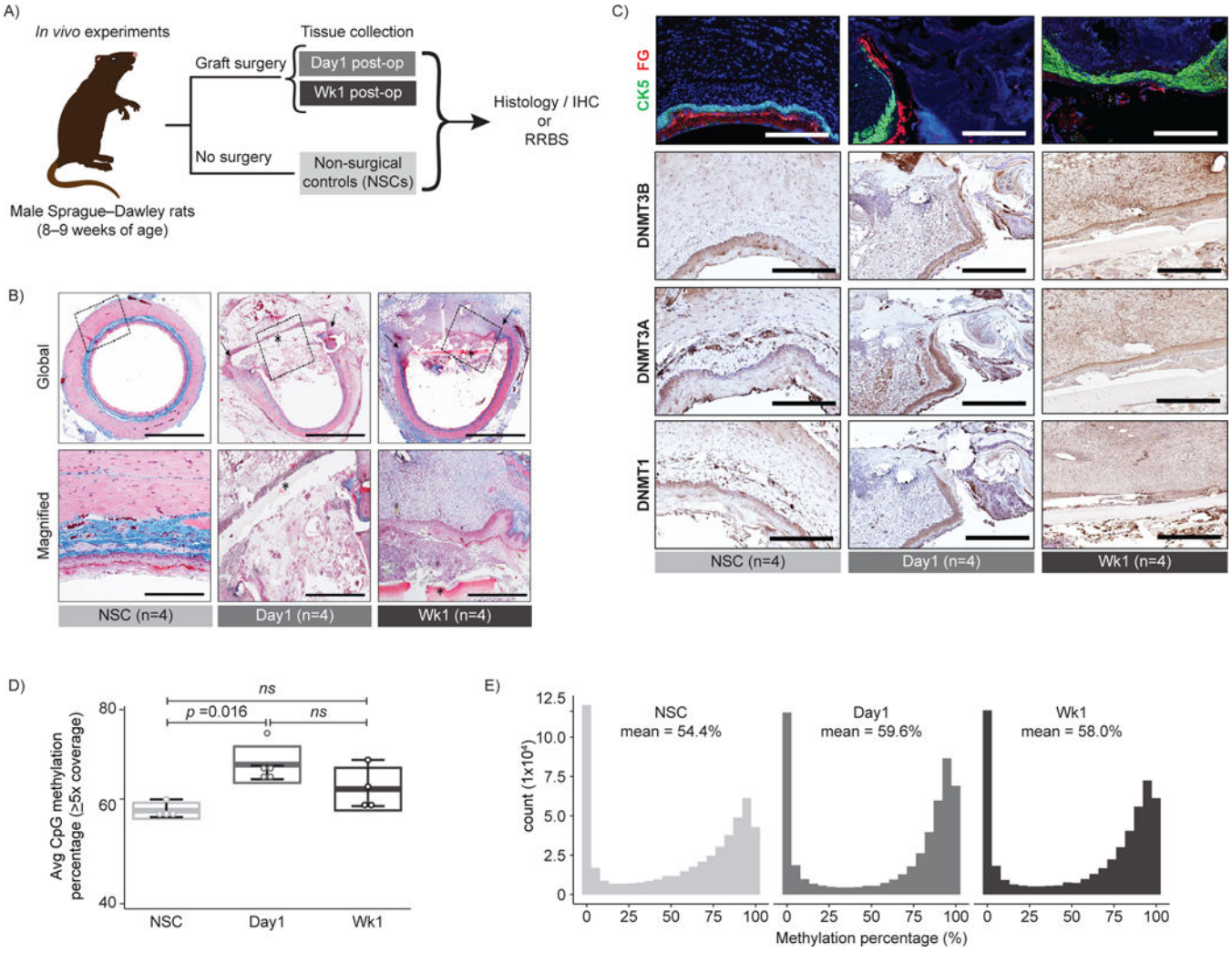

Figure 1. RRBS characterization of temporal DNA methylation dynamics during esophageal regeneration.

A) Schematic representation of the experimental setup. Timeline, experimental conditions, and corresponding controls are shown. For RRBS, non-surgical controls (NSCs. n=4), Day1 (n=5), and Wk1 (n=5). For histological and immunohistochemical (IHC) analyses, NSCs (n=4), Day1 (n=4), and Wk1 (n=4). B) Masson's trichrome staining of reconstructed esophageal tissues was performed to temporally characterize early phases of tissue regeneration and host tissue responses during the scaffold implantation period (n=4 for each condition). Arrows denote anastomotic borders of the implant site and asterisks denote residual scaffold fragments. C) Top: Representative images of NSC and neotissues supported by acellular grafts demonstrating protein expression of cytokeratin (CK)5 and filaggrin (FG) expression in red (FG) or green (CK5) while DAPI nuclear counterstain is detailed in blue. Cyan coloring is a consequence of merging CK5 and DAPI staining. IHC profiling of DNMT1, 3A, and 3B protein expression in NSC and in reconstructed host tissues at Day1 and Wk1 after surgery with counterstain. For all panels, images are representative of four biological replicates (n=4 for each condition). Scale bars = 200 μm. D) Boxplot displaying the mean genome-wide CpG methylation percentage using the average number of CpG

captured with ≥5x coverage in each condition: NSC (n=3,311,677), Day1 (n=2,708,305), and Wk1 (n=13,610,699) for NSC (n=4), Day1 (n=5), and Wk1 (n=4) biological replicates. Boxplots indicate the mean (middle thicker line) and interquartile range (outer box) of NSC (n=4), Day1 (n=5), and Wk1 (n=4) independent biological replicates. The *p*-values were calculated using Wilcoxon rank-sum test. *ns* indicates $p > 0.05$. E) Histograms displaying the distribution of CpG methylation percentage in each experimental group for CpGs (≥5x depth) that were captured in at least 3 replicates in each experimental group (n=514,813) for NSC (n=4), Day1 (n=4), and Wk1 (n=4) biological replicates.

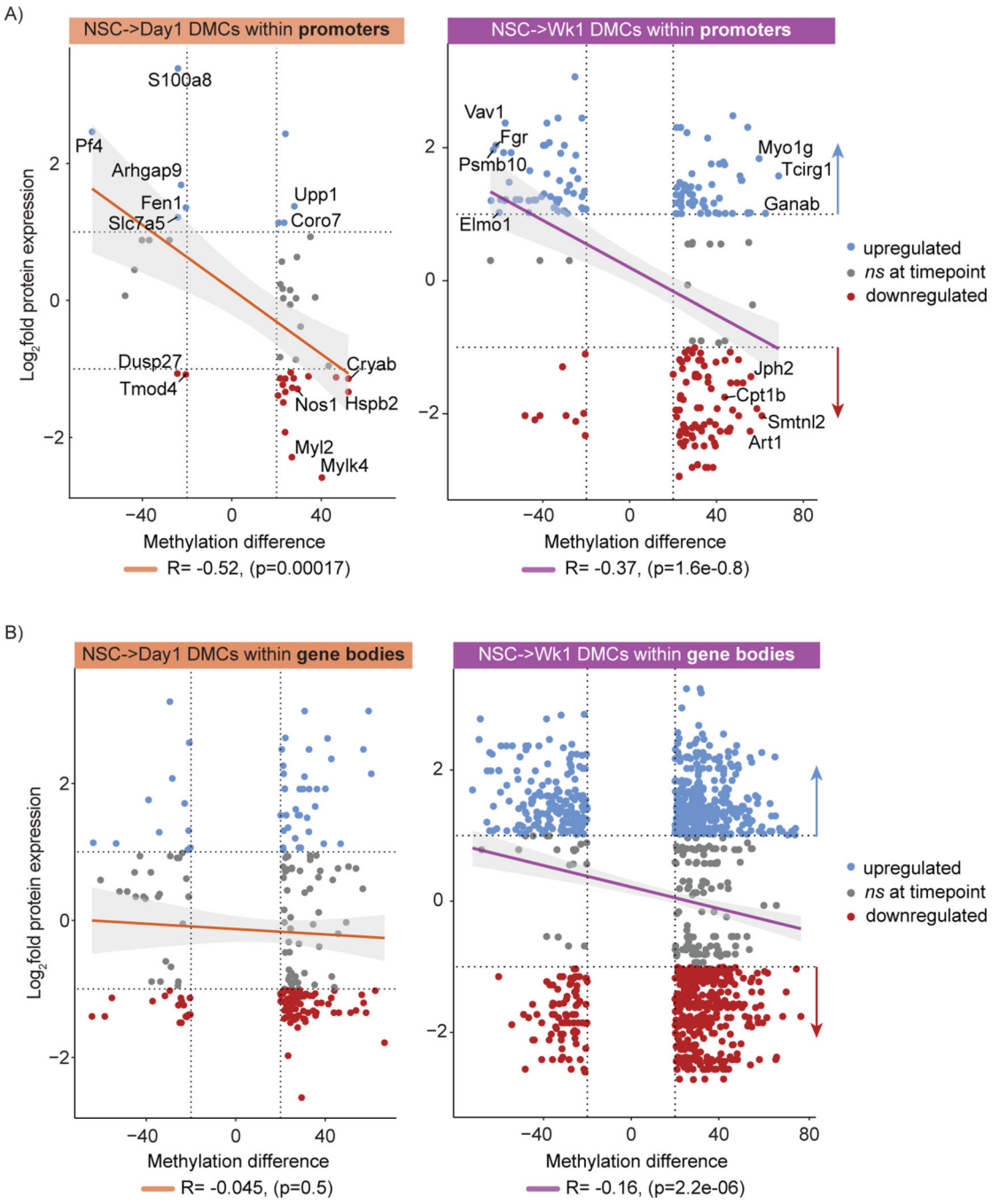

Figure 2. CpG methylation levels are inversely correlated with DEP expression levels during regeneration.

A) Left: Scatterplot displaying the methylation difference for NSC→Day1 DMCs that fall within promoters, as well as the log_2fold protein expression value for the protein encoded by the gene associated with that DMC. Orange line represents linear regression and gray shading represents 95% confidence interval. Right: Scatterplot displaying the methylation difference for NSC→Wk1 DMCs that fall within promoters, as well as the log_2fold protein expression value for the protein encoded by the gene associated with that DMC. Violet line represents linear regression and gray shading represents 95% confidence interval. Dotted

horizontal lines represent log_2fold protein expression value of 1 and −1. Dotted vertical lines represent 20% methylation difference threshold for calling DMCs. The average log_2fold protein expression of DEPs which were previously identified in post-surgical timepoints compared to the NSC for biological replicates (4 for each condition). The proteomics data was obtained from Gundogdu et al. Sci Reports. 2021.[8] B) Left: Scatterplot displaying the methylation difference for NSC→Day1 DMCs that fall within gene bodies, as well as the log_2fold protein expression value for the protein encoded by the gene associated with that DMC. Orange line represents linear regression and gray shading represents 95% confidence interval. Right: Scatterplot displaying the methylation difference for NSC→Wk1 DMCs that fall within gene bodies, as well as the log_2fold protein expression value for the protein encoded by the gene associated with that DMC. Violet line represents linear regression and gray shading represents 95% confidence interval. Dotted horizontal lines represent log_2fold protein expression value of 1 and −1. Dotted vertical lines represent 20% methylation difference threshold for calling DMCs. The average log_2fold protein expression of DEPs which were previously identified in post-surgical timepoints compared to the NSC for biological replicates (4 for each condition) (n=1,506 DEPs). The proteomics data was obtained from Gundogdu et al. Sci Reports. 2021.[8]

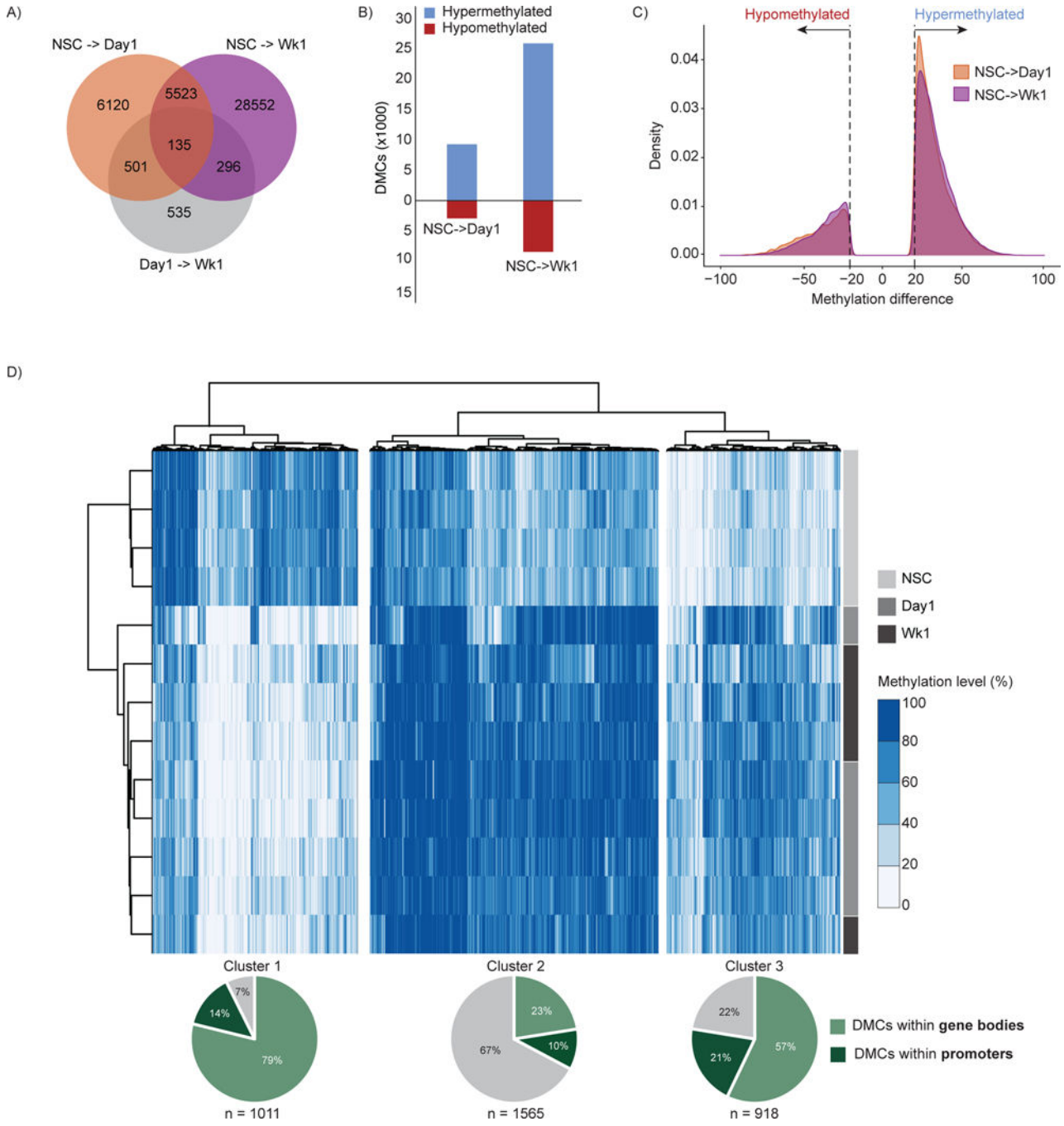

Figure 3. DNA hypermethylation is largely observed at post-surgical repair timepoints.

A) Venn diagram displaying shared and unique DMCs called among the comparison groups: NSC→Day1 (DMCs called at Day1 relative to NSC baseline), NSC→Wk1 (DMCs called at Wk1 relative to NSC baseline), Day1Wk1 (DMCs called at Wk1 relative to Day1). DMCs were called at a threshold of 20% CpG methylation difference and q-value<0.01. The number of DMCs for each group comparison: NSC→Day1 (n=12,279), NSC→Wk1 (n=34,506) and Day1Wk1(1,467). B) Bar plot showing the number of hypermethylated and hypomethylated DMCs in each comparison group. The number of hypermethylated

DMCs for the NSC→Day1 (n=9,247) and NSC→Wk1 (25,945) groups. The number of hypomethylated DMCs for the NSC→Day1 (n=3,032) and NSC→Wk1 (8,561) groups. C) Density plot depicting the distribution of hypermethylated and hypomethylated DMCs in each comparison group. D) Top: For shared DMCs that are represented in each individual sample with ≥5x coverage (n=3,494), corresponding CpG methylation levels within in each sample are shown in the heatmap. Euclidean hierarchical clustering was performed with pHeatmap package (version 1.0.12) using the ward.D2 clustering method in RStudio (version 4.0.5). Three clusters with different temporal DNA methylation dynamics were identified. Bottom: Pie charts displaying the distribution of DMCs corresponding to each cluster that fall within a gene body, promoter, or neither.

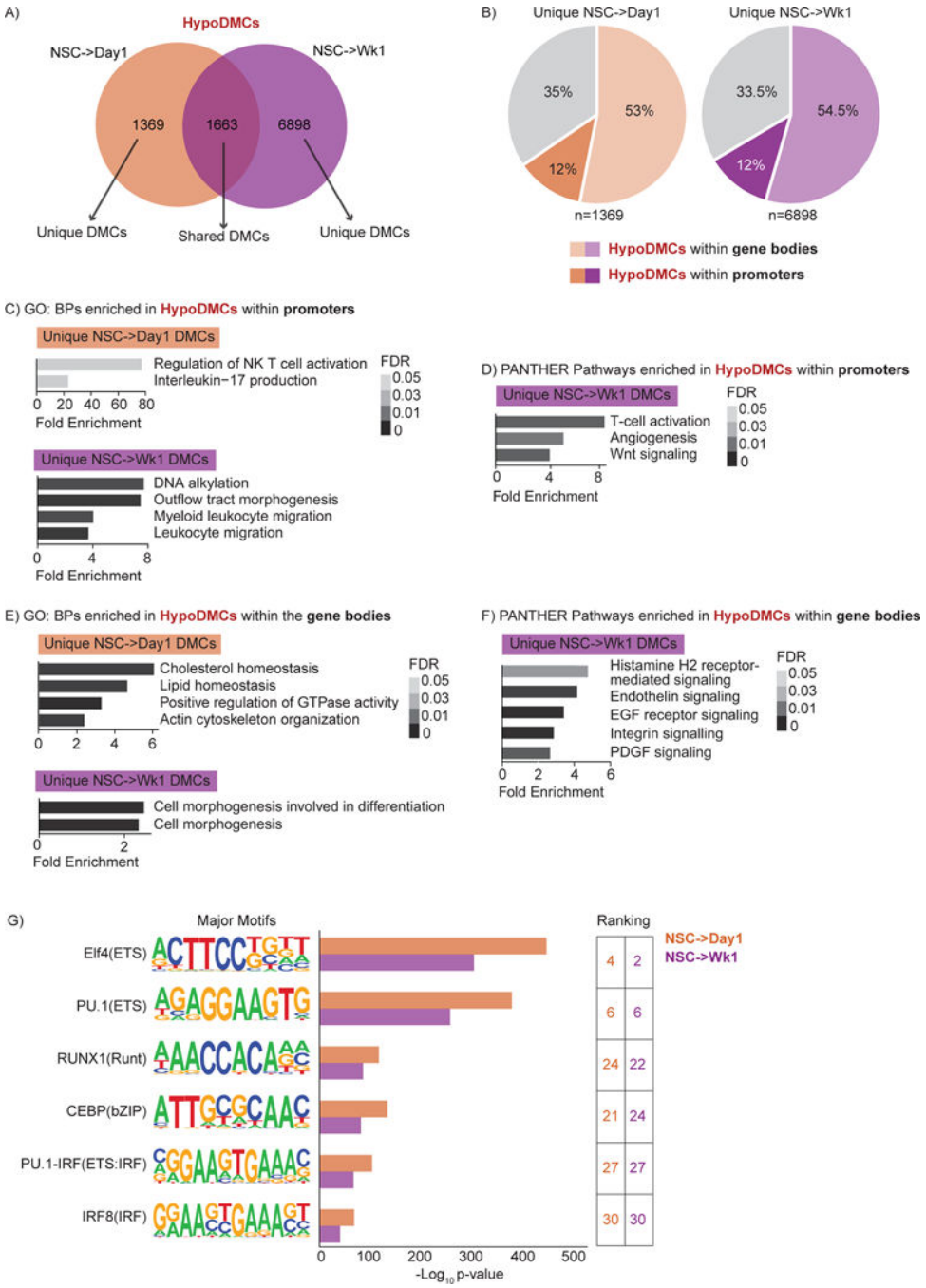

Figure 4. Hypomethylation occurs at CpG sites found in promoters of genes associated with immune activation.

A) Venn diagram displaying shared and unique hypomethylated DMCs (HypoDMCs) between NSC→Day1 (n=3,032) and NSC→Wk1 (n=8,561) groups. B) Pie charts showing the proportions of unique HypoDMCs located within gene bodies, promoters, or neither for NSC→Day1 and NSC→Wk1 comparison groups. Panels C-F) Plots depicting enriched GO: biological processes (BPs) and PANTHER pathways. The x-axis indicates fold enrichment and the colors indicate the false-discovery rate (FDR). C) Bar plot depicting GO: (BPs) enriched for genes associated with HypoDMCs found within promoters that are unique

to NSC→Day1 (top) or that are unique to NSC→Wk1 (bottom). 132 and 550 genes were associated with unique NSC→Day1 and NSC→Wk1 HypoDMCs within promoters, respectively. (D) Bar plot depicting PANTHER pathways enriched for genes associated with HypoDMCs found within promoters that are unique to NSC→Wk1. No PANTHER pathways were significantly enriched for the genes associated with unique NSC→Day1 HypoDMCs found within promoters. E) Bar plot depicting GO: BPs enriched for genes associated with HypoDMCs found within gene bodies that are unique to NSC→Day1 (top) or that are unique to NSC→Wk1 (bottom). 539 and 2,073 genes were associated with unique NSC→Day1 and NSC→Wk1 HypoDMCs within gene bodies, respectively. F) Bar plot depicting PANTHER pathways enriched for genes associated with HypoDMCs found within gene bodies that are unique to NSC→Wk1. No PANTHER pathways were significantly enriched for the genes associated with unique NSC→Day1 HypoDMCs found within gene bodies. G) Transcription factor binding motifs enriched for unique NSC→Day1 and NSC→Wk1 HypoDMCs. Motif logos are shown in the left column. Bar plot shows the degree of statistical significance for each motif enrichment. Motifs were ranked by $-\log_{10}(p\text{-values})$ in each condition calculated by HOMER.

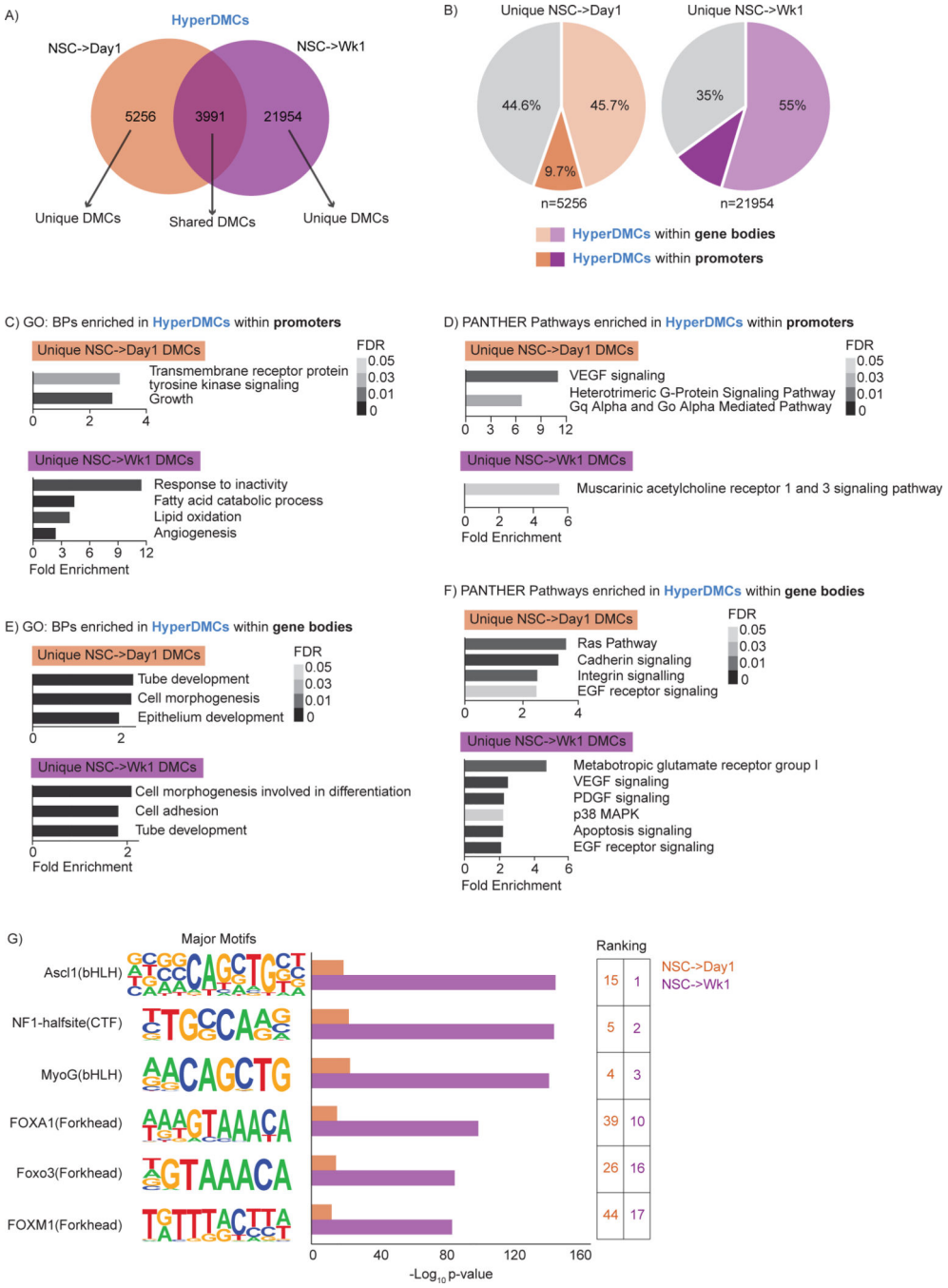

Figure 5. Hypermethylation at post-surgical repair timepoints targets genes involved in PI3K-Akt signaling.

A) Venn diagram displaying shared and unique hypermethylated DMCs (HyperDMCs) between NSC→Day1 (n=9,247) and NSC→Wk1 (n=25,945) groups. B) Pie charts showing the proportions of unique HyperDMCs located within gene bodies, promoters, or neither for NSC→Day1 and NSC→Wk1 comparison groups. Panels C-F) Plots depicting enriched GO: biological processes (BPs) and PANTHER pathways. The x-axis indicates fold enrichment and the colors indicate the false-discovery rate (FDR). C) Bar plot depicting GO: (BPs) enriched for genes associated with HyperDMCs found within promoters that are unique

to NSC→Day1 (top) or that are unique to NSC→Wk1 (bottom). 460 and 1,438 genes were associated with unique NSC→Day1 and NSC→Wk1 HyperDMCs within promoters, respectively. D) Bar plot depicting PANTHER pathways enriched for genes associated with HyperDMCs found within promoters that are unique to NSC→Day1 (top) or that are unique to NSC→Wk1 (bottom). E) Bar plot depicting GO: BPs enriched for genes associated with HyperDMCs found within gene bodies that are unique to NSC→Day1 (top) or that are unique to NSC→Wk1 (bottom). 1,715 and 4,999 genes were associated with unique NSC→Day1 and NSC→Wk1 HyperDMCs within gene bodies, respectively. F) Bar plot depicting PANTHER pathways enriched for genes associated with HyperDMCs found within gene bodies that are unique to NSC→Day1 (top) or that are unique to NSC→Wk1 (bottom). G) Transcription factor binding motifs enriched for unique NSC→Day1 and NSC→Wk1 HyperDMCs. Motif logos are shown in the left column. Bar plot shows the degree of statistical significance for each motif enrichment. Motifs were ranked by $-\log_{10}(p\text{-values})$ in each condition calculated by HOMER.

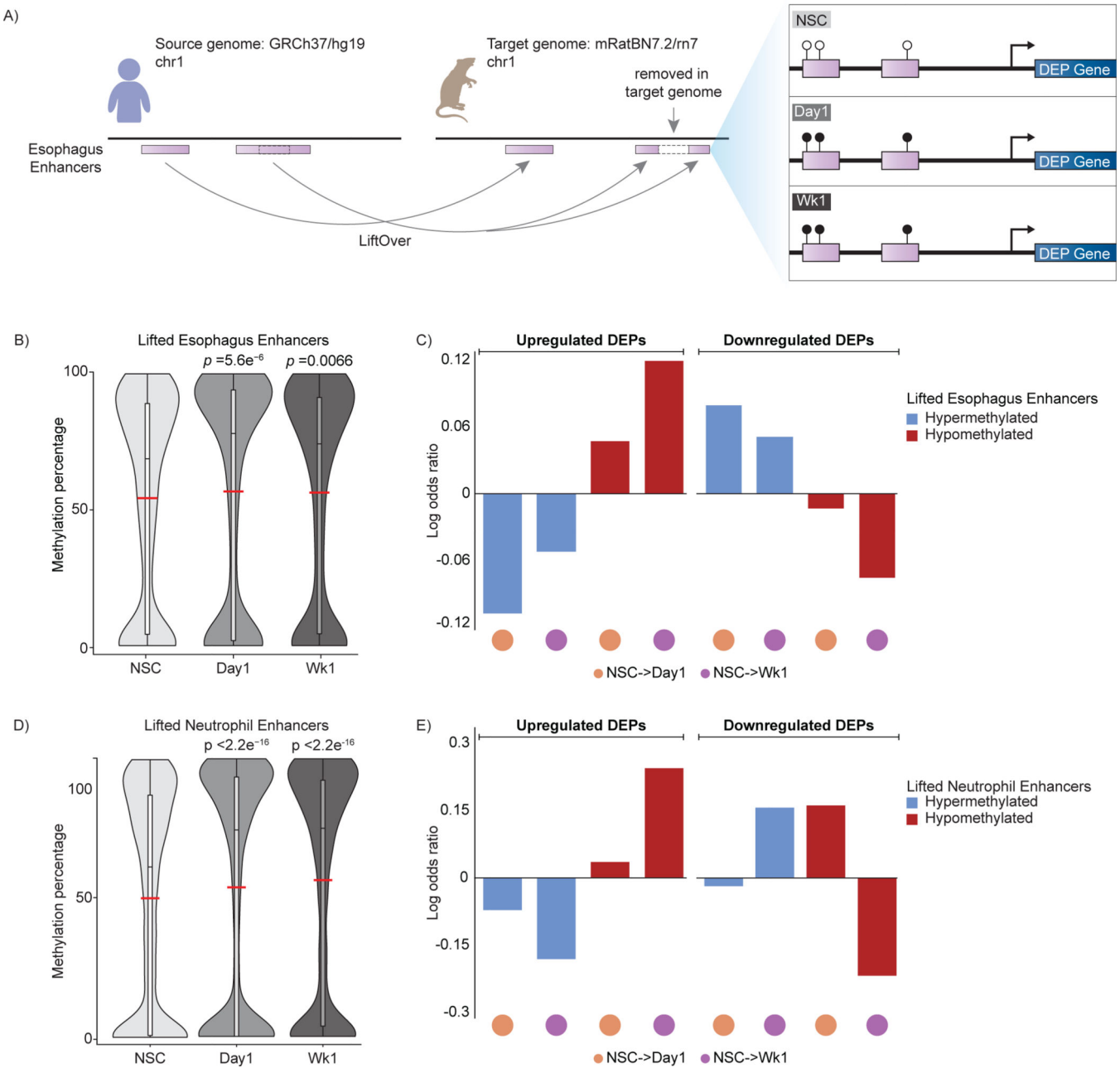

Figure 6. Conserved enhancer regions exhibit differential methylation that is associated with differentially expressed proteins showed content specific trends between the two timepoint comparisons.

A) Schematic illustration of experimental workflow for characterizing methylation changes in conserved genomic regions between GRCh37/hg19 and mRatBN7.2/rn7 genomes. Black circles represent methylated CpGs, while white circles represent unmethylated CpGs. In this scenario, the enhancer of interest is hypermethylated at Day1 and Wk1 compared to the NSC. B) Violin plots depicting the distribution of CpG methylation percentage for all CpGs within lifted esophagus enhancers (n=13,189) for each experimental timepoint. The *p*-values were calculated with Wilcoxon rank-sum test. C) Bar plots show the logOR between

differentially methylated lifted esophagus enhancers that were hypomethylated (red) and hypermethylated (blue) and DEPs for each timepoint comparison. The colored circles at the bottom reflect timepoint comparisons (i.e., orange indicates NSC Day1 and violet indicates NSC→Wk1). LogOR significance was calculated with Fisher's exact test. Note: LogOR were *ns*. D) Violin plots depicting the distribution of CpG methylation percentage for all CpGs within lifted neutrophil enhancer regions (n=11,294) for each experimental timepoint. The *p*-values were calculated with Wilcoxon rank-sum test. E) Bar plots show the logOR between differentially methylated lifted neutrophil enhancers that were hypomethylated (red) and hypermethylated (blue) and DEPs for each timepoint comparison. The colored circles at the bottom reflect timepoint comparisons (i.e., orange indicates NSC Day1 and violet indicates NSC→Wk1). LogOR significance was calculated with Fisher's exact test. Note: LogOR were *ns*.